Ann. N.Y. Acad. Sci. ISSN 0077-8923

ANNALS OF THE NEW YORK ACADEMY OF SCIENCES
Issue: *Barriers and Channels Formed by Tight Junction Proteins*

Claudin-based paracellular proton barrier in the stomach

Atsushi Tamura,[1] Yuji Yamazaki,[1] Daisuke Hayashi,[1,2] Koya Suzuki,[1] Kazuhiro Sentani,[3] Wataru Yasui,[3] and Sachiko Tsukita[1]

[1]Laboratory of Biological Science, Graduate School of Frontier Biosciences and Graduate School of Medicine, Osaka University, Osaka, Japan. [2]Department of Geriatric Medicine and Nephrology, Graduate School of Medicine, Osaka University, Osaka, Japan. [3]Department of Molecular Pathology, Graduate School of Biomedical Sciences, Hiroshima University, Hiroshima, Japan

Address for correspondence: Sachiko Tsukita, Laboratory of Biological Science, Graduate School of Frontier Biosciences, Osaka University, 2-2 Yamadaoka, Suita, Osaka 565-0871, Japan. atsukita@biosci.med.osaka-u.ac.jp

The claudins comprise a multigene family that consists of at least 27 members. Claudins are responsible for establishing the paracellular barrier—which has permselectivity—at the tight junctions in epithelial cells, and the specific patterns of claudin expression in the epithelial cell sheets that cover the internal and external surfaces of organs contribute to the formation of microenvironments and organs' biological functions. Data on the detailed characterization of individual claudins and their roles in different microenvironments are accumulating. A study on the stomach-specific *claudin-18*–knockout mouse, which has gastritis, recently revealed that the stomach-type claudin-18 specifically forms the proton barrier in the stomach, consistent with previously reported circumstantial evidence. Combined with previous studies on the specific ionic homeostasis by different types of claudins, our findings support the idea that claudins may regulate ion-specific homeostasis *in vivo*.

Keywords: claudin; proton barrier; gastritis; knockout mouse; metaplasia

Biological significance of the large claudin family

Since the first claudin was identified as a tight-junction protein, the claudin family has been shown to include a large number of members, at least 27, in humans and mice (Fig. 1A).[1–3] Why the claudin family is so large is an important question. Given that claudins form the paracellular barrier in various types of epithelial cell sheets in different organs *in vivo*, the many species of claudin are probably important to confer different epithelial cell–sheet barrier properties, including barrier-dependent permselectivity, thereby establishing microenvironments in specific regions of individual organs.[4–7] Together with the specific properties of claudins determined by cell-level analyses, critical roles for claudins *in vivo* have recently been revealed by studying knockout mice and human claudin genes that are mutated in various diseases.[8–10]

Studies involving the transfection or knockdown of individual claudins or their combinations in cultured epithelial cells led us and others to speculate that claudin-2, -10b, and -15 contribute to cation channels or pores, whereas claudin-4, -7, and -10a contribute to anion channels or pores or to cation barriers.[2,10–14] The positive or negative electrical charges of the first loops of a claudin molecule appear to function in paracellular epithelial permeation by creating an ion-channel like pore.[10,14] On the other hand, the dynamic properties of tight junctions (TJs) may determine the paracellular permeability for solutes, the mechanism of which is not well understood.[12,15–17]

Mutational analyses of human claudin genes have suggested that neonatal sclerosing cholangitis and icthyosis are caused by a *claudin-1* mutation.[15,18] Nonsyndromic recessive deafness is attributable to a *claudin-14* mutation, which causes dysfunction of the paracellular permselectivity of the inner ear epithelia.[19] Familiar hypomagnesemia is caused by a *claudin-16* mutation, which results in dysfunction of the cation permselectivity of the renal epithelia and familial hypomagnesemia,

doi: 10.1111/j.1749-6632.2012.06570.x

Ann. N.Y. Acad. Sci. 1258 (2012) 108–114

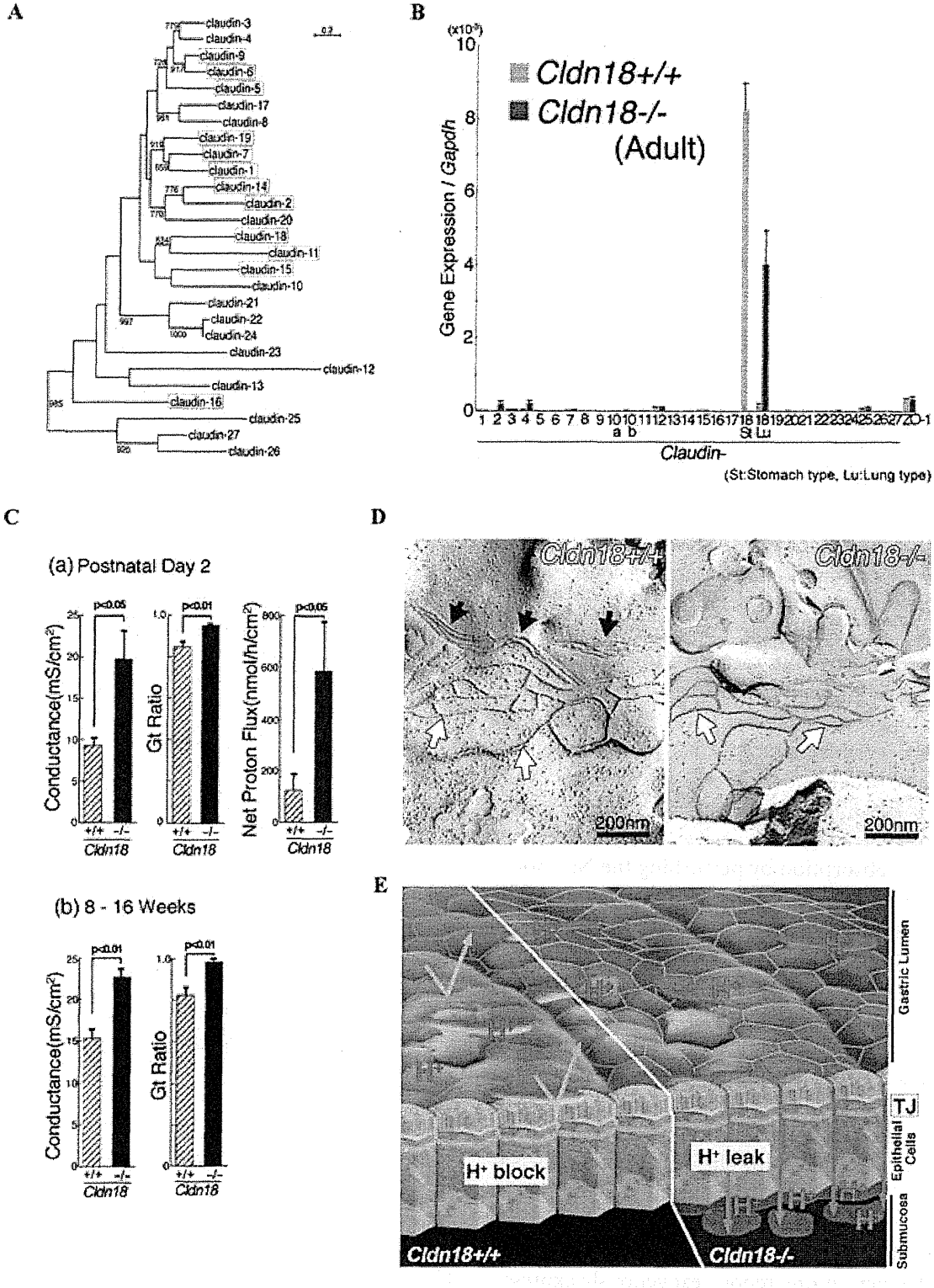

Figure 1. Claudin-18st forms a paracellular proton barrier. (A) The phylogenic relationship of 27 claudin-family members. The boxed claudins are those that have been analyzed in knockout mice for their biological significance *in vivo*. (B) The specific loss of *claudin-18st* in the *Cldn18*$^{-/-}$ stomach. Quantitative RT-PCR. (C) Physiological characterization of the transepithelial conductance and paracellular proton barrier in the *Cldn18*$^{+/+}$ stomach and its loss in the *Cldn18*$^{-/-}$stomach. The Gt ratio was obtained by dividing the conductance after acid-loading by the conductance before acid-loading. (D) Freeze-fracture electron microscopic images of TJ strands in the *Cldn18*$^{+/+}$ and *Cldn18*$^{-/-}$ stomach. Densely packed TJ strands (black arrows) in the apical region of the *Cldn18*$^{+/+}$ gastric epithelial cells were missing in the *Cldn18*$^{-/-}$ cells, which showed only loosely anastomosing TJ strands (white arrows). (E) Schematic illustrating the loss of the paracellular proton barrier by claudin-18st deficiency.

hypercalciuria and nephrocalcinosis (FHHNC).[20] FHHNC is reportedly caused by a *claudin-19* mutation.[21,22] These findings suggest that claudins are important determinants of specific homeostatic properties.[7–9] Knockout mice can be a powerful tool in clarifying the relationship between the function of claudins in TJs and biological homeostasis *in vivo*.[23,24]

The role of claudins as regulators of homeostasis as revealed by knockout mouse studies

The phenotypes of claudin knockout mice have revealed important roles for specific claudins in regulating the barrier integrity of certain epithelial tissues. For example, *claudin-1* knockout mice die shortly after birth due to disruption of epidermal barrier function and resultant dehydration. In *claudin-5* knockout mice, neonatal lethality is attributable to the disruption of endothelial barrier integrity in the central nervous system and the resultant loss of blood–brain barrier function.[25,26] *Claudin-11* knockout mice are viable, but they have locomotion defects and male sterility due, respectively, to a lack of TJs in the myelin sheaths of the central nervous system, which affects nerve conduction, and between Sertoli cells of the testes, which affects the blood–testis barrier.[27] The knockout of ion-leaky *claudin-15* causes defects in nutrition absorption by perturbing the Na^+ homeostasis that is required for the proper functioning of nutrition absorption transporters.[24] Thus, the claudin-type–specific properties of a permselective paracellular barrier help regulate the homeostasis of different biological systems. Detailed studies of these systems should reveal the mechanisms by which claudins regulate the homeostasis of each microenvironment.

The ion permselectivity of paracellular barriers, and particularly of the permeability to Na^+, K^+, $Mg2^+$, and Cl^-, have been intensively analyzed.[2,24,28,29] Findings in studies of cultured cells suggest that claudins are involved in the proton (H^+) barrier. In one report, exogenously expressed claudin-8 conferred a proton barrier property on MDCK-2 cells; in another, exogenously expressed claudin-18 conferred the ability for cells to form a proton barrier between them.[29,30]

Furthermore, the expression of stomach type of *claudin-18 (claudin-18st)* is upregulated in human Barrett's esophagus, which might contribute to the high proton barrier seen in this disorder.

The proton-barrier property of claudin-18st, a dominant claudin in the stomach, is thought to be especially important *in vivo* to prevent H^+ leakage from acidic gastric juice into the tissues. To uncover the role of this claudin *in vivo*, we recently generated and analyzed *claudin-18st* knockout mice.[31]

Claudin-18 is a proton paracellular barrier protein in the stomach

We first examined which claudins are expressed in the mouse stomach by qRT-PCR. As shown in Figure 1B, many claudins are expressed in the stomach, but the expression level of *claudin-18* is exclusively high. *Claudin-18* has two alternative splicing forms, the stomach (type 2 splicing form, designated as *claudin-18st* in this manuscript) and lung (type 1 splicing form) types, which use different first exons and the same exons 2–4. The two isoforms are regulated by different tissue-specific promotors.[32] The stomach-type *claudin-18* is thought to regulate the H^+-leakage resistance of the stomach's paracellular barrier. To examine this possibility, we recently generated and analyzed knockout mice of stomach-type claudin-18 ($Cldn18^{-/-}$mice).

The epithelial paracellular barrier function against H^+ was examined in the stomach of $Cldn18^{+/+}$ and $Cldn18^{-/-}$ mice. Electrophysiological measurements showed that the total ion permeability (conductance) for the buffer containing 150 mM NaCl was higher in the $Cldn18^{-/-}$ stomach than the $Cldn18^{+/+}$ one, suggesting that the claudin-18 deficiency compromised the total paracellular ionic barrier. While the paracellular barrier against acidity was effective in the $Cldn18^{+/+}$ stomach, this was not the case for the $Cldn18^{-/-}$ stomach, suggesting that the H^+ leakage was much lower in the $Cldn18^{+/+}$ stomach compared to $Cldn18^{-/-}$ one. These findings are consistent with the idea that claudin-18st plays a specific role in the paracellular barrier of the stomach to block H^+ leakage (Fig. 1C).

The mode of claudin-18st polymerization creates the gastric proton barrier

The formation of TJ strands, which can be revealed by freeze-fracture electron microscopy, is required for TJs to exert their paracellular barrier function.

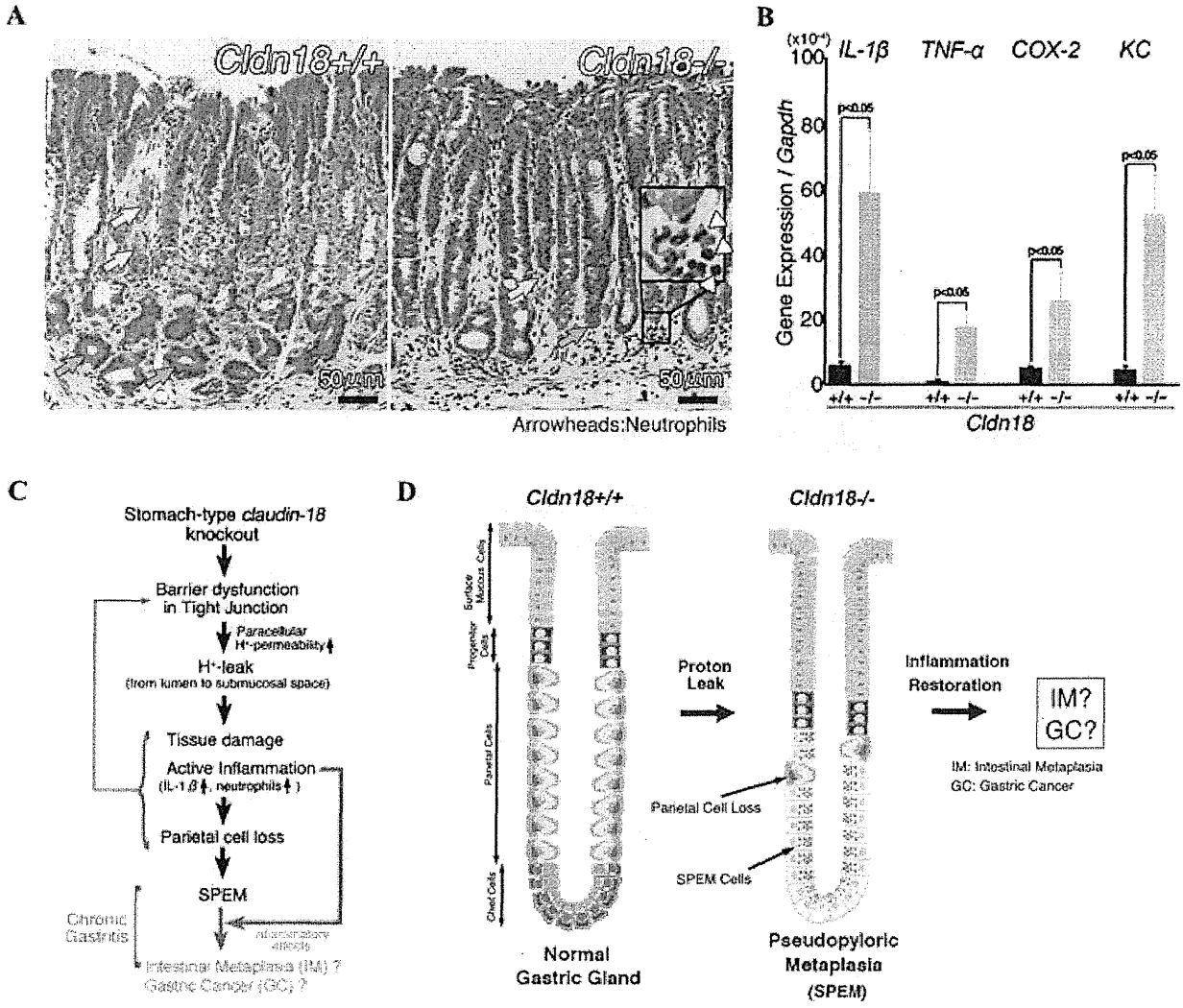

Figure 2. Characterization of the gastritis in the *Cldn18*$^{-/-}$ mice. (A) HE-stained preparations of *Cldn18*$^{+/+}$ and *Cldn18*$^{-/-}$ stomach tissue. Gastritis was recognized in the *Cldn18*$^{-/-}$ stomach, in which parietal and chief cells (yellow and pink arrows, respectively) were decreased. Note the presence of neutrophils that had infiltrated the submucosa in the *Cldn18*$^{-/-}$ stomach (white arrows in enlarged (×3.3) photographs in the inset). (B) Expressions of inflammatory cytokines IL-1β, TNF-α, COX-2, and KC in the *Cldn18*$^{+/+}$ and *Cldn18*$^{-/-}$ stomach. The cytokine expressions were upregulated in the *Cldn18*$^{-/-}$ stomach compared to the *Cldn18*$^{+/+}$ one. (C and D) Schematics showing the process of gastritis onset in the *Cldn18*$^{-/-}$ mouse stomach. Proton leakage due to dysfunctional tight junctions may trigger pseudopyloric gastritis in the *Cldn18*$^{-/-}$ stomach, with IL-1β–related inflammation.

As it is generally thought that the TJ-strand morphology at least partly reflects TJ function, we next investigated the TJ strands in the *Cldn18*$^{-/-}$ stomach using freeze-fracture electron microscopy (Fig. 1D). Tightly packed parallel arrays of TJ strands exist in the adult *Cldn18*$^{+/+}$ stomach, and these structures were lost in the *Cldn18*$^{-/-}$ stomach, suggesting that these arrays reflect the TJ paracellular proton barrier (Fig. 1E). In contrast, the stomach of the *Cldn18*$^{-/-}$ mouse showed much more loosely anastomosing TJ strands, which probably contained claudin species other than claudin-18st. An important future research goal is to determine the unique mode of claudin-18st polymerization that creates the proton paracellular barrier.

Biological significance of the claudin-18st paracellular proton barrier in the stomach

Although *Cldn18*$^{-/-}$ mice grow up without gross abnormalities compared to *Cldn18*$^{+/+}$ mice, tissue-level examination revealed a critical biological effect of claudin-18st *in vivo*: adult *Cldn18*$^{-/-}$ mice have chronic gastritis. Compared to *Cldn18*$^{+/+}$,

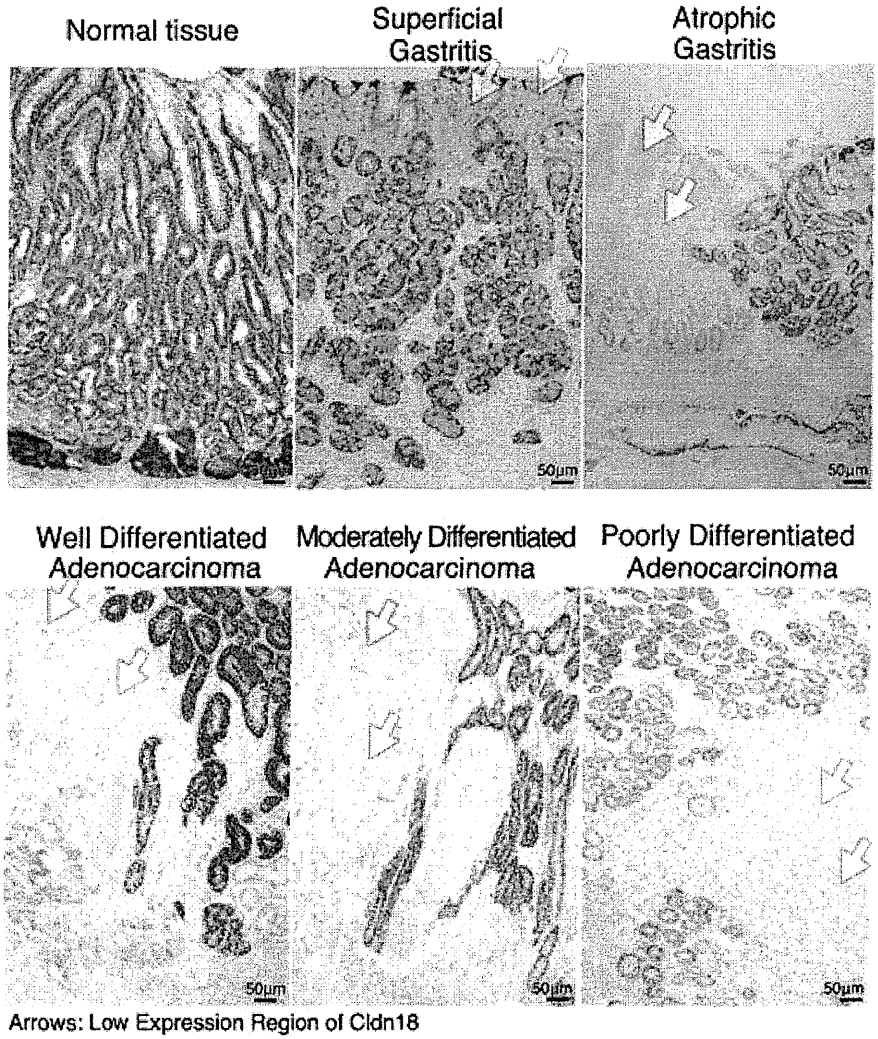

Figure 3. Human samples showing the downregulation of stomach-type claudin-18 in gastritis and gastric cancer. Immunohistochemically claudin-18–stained micrographs of paraffin sections of a normal stomach, stomachs with gastritis, and gastric cancer. Claudin-18 was downregulated in the gastritis and gastric cancer samples.

HE-stained *Cldn18*$^{-/-}$ stomach tissue revealed fewer parietal and chief cells, which had largely been replaced by metaplastic cells (Fig. 2A). Furthermore, inflammatory cells had infiltrated the *Cldn18*$^{-/-}$ submucosal space. Thus, the claudin-18st-based paracellular proton barrier protects the stomach against atrophic inflammation triggered by the undesired leakage of protons into the gastric submucosa.

We next examined the characteristics of the gastritis in the *Cldn18*$^{-/-}$ mice in detail. We found that the levels of proinflammatory cytokines including IL-1β (but not IL-6) and the neutrophil chemoattractant KC were significantly higher in the *Cldn18*$^{-/-}$ stomach than the *Cldn18*$^{+/+}$ stomach, by qRT-PCR (Fig. 2B). The serum protein level of IL-1β was also significantly upregulated in the *Cldn18*$^{-/-}$ mice. Analysis of the immune cell types by FACS revealed that neutrophils, which are positive for Gr-1, predominated in the gastritic *Cldn18*$^{-/-}$ tissue. This is in agreement with our HE staining and immunofluorescence images showing that neutrophils were significantly increased in the stomach of younger adult *Cldn18*$^{-/-}$ mice examined (< 20 weeks old).

Claudin-18st and gastric metaplasia in mice

In the *Cldn18*$^{-/-}$ mouse stomach, the gastric epithelium was largely occupied by proliferating mucous-like cells that were positive for trefoil factor family 2 (TFF2). Some of these cells

were also positive for intrinsic factor, indicating that they were spasmolytic polypeptide-expressing metaplastic (SPEM) cells.[33] Although several reports have shown that SPEM cells are associated with >90% of gastric cancers, neither dysplasia nor gastric cancer was found in the stomach of younger *Cldn18*$^{-/-}$ mice (<20 weeks old).[33,34] On the other hand, other chronic inflammation markers such as IL-6 were sporadically upregulated in *Cldn18*$^{-/-}$ mice (Suzuki *et al.*, unpublished data), hinting at a relationship between the claudin-18st–based SPEM and dysplasia/cancer (Fig. 2C and D).

Claudin-18 and gastritis and gastric cancer in humans

Since previous studies reported that claudin-18 expression is downregulated in human gastric cancer, we also investigated the expression levels of claudin-18 in human chronic and autoimmune gastritis by immunohistochemical methods. Claudin-18 was found to be downregulated in human gastritis specimens, at foci that showed atrophy and metaplasia. In superficial gastritis, the claudin-18 level was also decreased. Thus, it would appear that claudin-18 is downregulated pathologically in human gastritis as it is in gastric cancer (Fig. 3). These findings point to the possibility that claudin-18 loss induces gastritis, which creates a setting for dysplasia and/or cancer. This finding leads to important questions on the role of claudins in cancer that will be addressed in future research.

Summary

Given the conceptual consensus that the large multigene claudin family plays a critical role in creating various microenvironments in organ systems, particular attention is being paid to effects of claudin-based regulation of paracellular barriers and the barrier-based ion permeability between epithelial cells on homeostasis *in vivo*. We recently showed that claudin-18 forms the paracellular proton barrier that prevents gastritis in the stomach. Further studies will be focused on revealing the function of claudins in metaplasia, dysplasia, and cancer. As other claudins also regulate biological functions, further analyses at the cellular level and on the *in vivo* functions of claudin-family proteins should elucidate the physiological significance of claudin-family members in various biological systems.

Conflicts of interest

The authors declare no conflicts of interest.

References

1. Tsukita, S., M. Furuse & M. Itoh. 2001. Multifunctional strands in tight junctions. *Nat. Rev. Mol. Cell Biol.* **2:** 285–293.
2. Van Itallie, C.M. & J.M. Anderson. 2006. Claudins and epithelial paracellular transport. *Annu. Rev. Physiol.* **68:** 403–429.
3. Mineta, K. *et al.* 2011. Predicted expansion of the claudin multigene family. *FEBS Lett.* **585:** 606–612.
4. Angelow, S., R. Ahlstrom & A.S. Yu. 2008. Biology of claudins. *Am. J. Physiol. Renal. Physiol.* **295:** F867–F876.
5. Fujita, H. *et al.* 2006. Differential expression and subcellular localization of claudin-7, -8, -12, -13, and -15 along the mouse intestine. *J. Histochem. Cytochem.* **54:** 933–944.
6. Holmes, J.L. *et al.* 2006. Claudin profiling in the mouse during postnatal intestinal development and along the gastrointestinal tract reveals complex expression patterns. *Gene Expr. Patterns* **6:** 581–588.
7. Soini, Y. 2011. Claudins in lung diseases. *Respir. Res.* **12:** 70.
8. Marchiando, A.M., W.V. Graham & J.R. Turner. 2010. Epithelial barriers in homeostasis and disease. *Annu. Rev. Pathol.* **5:** 119–144.
9. Gupta, I.R. & A.K. Ryan. 2010. Claudins: unlocking the code to tight junction function during embryogenesis and in disease. *Clin. Genet.* **77:** 314–325.
10. Van Itallie, C.M., A.S. Fanning & J.M. Anderson. 2003. Reversal of charge selectivity in cation or anion-selective epithelial lines by expression of different claudins. *Am. J. Physiol. Renal. Physiol.* **285:** F1078–F1084.
11. Amasheh, S. *et al.* 2002, Claudin-2 expression induces cation-selective channels in tight junctions of epithelial cells. *J. Cell Sci.* **115:** 4969–4976.
12. Furuse, M., K. Furuse., H. Sasaki & S. Tsukita. 2001. Conversion of zonulae occludentes from tight to leaky strand type by introducing claudin-2 into Madin-Darby canine kidney I cells. *J. Cell Biol.* **153:** 263–272.
13. Van Itallie C.M. *et al.* 2006. Two splice variants of claudin-10 in the kidney create paracellular pores with different ion selectivities. *Am. J. Physiol. Renal. Physiol.* **291:** F1288–F1299.
14. Yu, A.S. *et al.* 2009. Molecular basis for cation selectivity in claudin-2-based paracellular pores: identification of an electrostatic interaction site. *J. Gen. Physiol.* **133:** 111–127.
15. Sasaki, H. *et al.* 2003. Dynamic behavior of paired claudin strands within apposing plasma membranes. *Proc. Natl. Acad. Sci. USA* **100:** 3971–3976.
16. Madara, J.L. 1998. Regulation of the movement of solutes across tight junctions. *Annu. Rev. Physiol.* **60:** 143–159.
17. Shen, L. *et al.* 2011. Tight junction pore and leak pathways: a dynamic duo. *Annu. Rev. Physiol.* **73:** 283–309.
18. Hadj-Rabia, S. *et al.* 2004. Claudin-1 gene mutations in neonatal sclerosing cholangitis associated with ichthyosis: a tight junction disease. *Gastroenterology* **127:** 1386–1390.
19. Wilcox, E.R. *et al.* 2001. Mutations in the gene encoding tight junction claudin-14 cause autosomal recessive deafness DFNB29. *Cell* **104:** 165–172.

20. Weber, S. *et al.* 2000. Familial hypomagnesaemia with hypercalciuria and nephrocalcinosis maps to chromosome 3q27 and is associated with mutations in the PCLN-1 gene. *Eur. J. Hum. Genet.* **8:** 414–422.
21. Simon, D.B. *et al.* 1999. Paracellin-1, a renal tight junction protein required for paracellular $Mg2^{+}$ resorption. *Science* **285:** 103–106.
22. Naeem, M., S. Hussain & N. Akhtar. 2011. Mutation in the tight-junction gene claudin 19 (CLDN19) and familial hypomagnesemia, hypercalciuria, nephrocalcinosis (FHHNC) and severe ocular disease. *Am. J. Nephrol.* **34:** 241–248.
23. Anderson, J.M. & C.M. Van Itallie. 2009. Physiology and function of the tight junction. *Cold. Spring. Harb. Perspect. Biol.* **1:** a002584.
24. Tamura, A. *et al.* 2011. Loss of claudin-15, but not claudin-2, causes Na^{+} deficiency and glucose malabsorption in mouse small intestine. *Gastroenterology* **140:** 913–923.
25. Furuse, M. *et al.* 2002. Claudin-based tight junctions are crucial for the mammalian epidermal barrier: a lesson from claudin-1-deficient mice. *J. Cell Biol.* **156:** 1099–1111.
26. Nitta, T. *et al.* 2003. Size-selective loosening of the blood-brain barrier in claudin-5-deficient mice. *J. Cell Biol.* **161:** 653–660.
27. Gow, A. *et al.* 1999. CNS myelin and sertoli cell tight junction strands are absent in Osp/claudin-11 null mice. *Cell* **99:** 649–659.
28. Hou, J. *et al.* 2006. Study of claudin function by RNA interference. *J. Biol. Chem.* **281:** 36117–36123.
29. Angelow, S., K.J. Kim & A.S. Yu. 2006. Claudin-8 modulates paracellular permeability to acidic and basic ions in MDCK II cells. *J. Physiol.* **571:** 15–26.
30. Jovov, B. *et al.* 2007. Claudin-18: a dominant tight junction protein in Barrett's esophagus and likely contributor to its acid resistance. *Am. J. Physiol. Gastrointest. Liver Physiol.* **293:** G1106–G1113.
31. Hayashi, D. *et al.* 2012. Deficiency of claudin-18 causes paracellular $H(^{+})$ leakage, up-regulation of interleukin-1β, and atrophic gastritis in mice. *Gastroenterology* **142:** 292–304.
32. Niimi, T. *et al.* 2001. Claudin-18, a novel downstream target gene for the T/EBP/NKX2.1 homeodomain transcription factor, encodes lung-and stomach-specific isoforms through alternative splicing. *Mol. Cell Biol.* **21:** 7380–7390.
33. Weis, V.G. & J.R. Goldenring. 2009. Current understanding of SPEM and its standing in the preneoplastic process. *Gastric Cancer* **12:** 189–197.
34. Oshima, H. & M. Oshima. 2010. Mouse models of gastric tumors: Wnt activation and PGE2 induction. *Pathol. Int.* **60:** 599–607.

World Journal of Gastroenterology

Online Submissions: http://www.wjgnet.com/esps/
wjg@wjgnet.com
doi:10.3748/wjg.v18.i44.6468

World J Gastroenterol 2012 November 28; 18(44): 6468-6474
ISSN 1007-9327 (print) ISSN 2219-2840 (online)

BRIEF ARTICLE

Clinicopathological features of minute pharyngeal lesions diagnosed by narrow-band imaging endoscopy and biopsy

Takashi Kumamoto, Kazuhiro Sentani, Shiro Oka, Shinji Tanaka, Wataru Yasui

Takashi Kumamoto, Kumamoto Gastrointestinal Clinic, Hiroshima 730-0051, Japan
Kazuhiro Sentani, Wataru Yasui, Department of Molecular Pathology, Hiroshima University Graduate School of Biomedical Sciences, Hiroshima 734-8551, Japan
Shiro Oka, Shinji Tanaka, Department of Endoscopy, Hiroshima University Hospital, Hiroshima 734-8551, Japan
Author contributions: Kumamoto T designed the study and drafted the manuscript; Sentani K and Yasui W performed the histological assessment; Oka S and Tanaka S interpreted the data.
Correspondence to: Dr. Takashi Kumamoto, Director, Kumamoto Gastrointestinal Clinic, 1-5-2 Otemachi, Naka-ku, Hiroshima 730-0051, Japan. kumamoto-clinic@guitar.ocn.ne.jp
Telephone: +81-82-5440606 Fax: +81-82-5440377
Received: March 5, 2012 Revised: July 6, 2012
Accepted: July 18, 2012
Published online: November 28, 2012

Abstract

AIM: To evaluate the utility of magnified narrow-band imaging (NBI) endoscopy for diagnosing and treating minute pharyngeal neoplasia.

METHODS: Magnified NBI gastrointestinal examinations were performed by the first author. A magnification hood was attached to the tip of the endoscope for quick focusing. Most of the examinations were performed under sedation. Magnified NBI examinations were performed for all of the pharyngeal lesions that had noticeable brownish areas under unmagnified NBI observation, and an intrapapillary capillary loop (IPCL) classification was made. A total of 93 consecutive pharyngeal lesions were diagnosed as IPCL type Ⅳ and were suspected to represent dysplasia. Sixty-two lesions of approximately 1 mm in diameter were biopsied in the clinic, and 17 lesions with larger diameters were resected by endoscopic submucosal dissection (ESD) at the Hiroshima University Hospital. In addition to the histological diagnoses, the lesion diameters were microscopically measured in 45 of the 62 biopsies. Thirty-four of the 62 biopsied patients received endoscopic follow up.

RESULTS: Minute pharyngeal lesions were diagnosed in 93 of approximately 3000 patients receiving magnified NBI examinations at the clinic. Of the 93 patients with IPCL type Ⅳ lesions, 80 were men, and 13 were women. Fifty-six were drinkers, and 57 were smokers. Two had esophageal cancer. Twenty-one lesions were located on the posterior hypopharyngeal wall, and 72 lesions were located on the posterior oropharyngeal wall. All 93 lesions were flat and showed similar findings in the magnified and unmagnified NBI examinations. Although almost all of the IPCL type Ⅳ lesions showed faint redness when examined under white light, it was difficult to diagnose the lesions using only this technique because the contrast was weaker than that achieved in the NBI examinations. Of the 93 lesions, only 3 had diameters greater than 2.1 mm. Sixty-two lesions of approximately 1 mm were biopsied in the clinic, whereas 17 larger lesions were treated by ESD at the Hiroshima University Hospital. Of the 79 pharyngeal lesions that were biopsied or resected by ESD, 5 were histologically diagnosed as high-grade dysplasia, 39 were diagnosed as low-grade dysplasia, and 39 were determined to be non-dysplastic lesions. There were no cancerous lesions. Histologically, abnormal cell size variations and increased nuclear size were observed in all of the high-grade dysplasia lesions, while the incidence of these findings in the low-grade dysplasia lesions was low. Of the 62 biopsied lesions, 45 were microscopically measurable. The measured diameters ranged from 0.1 to 2.0 mm. The dysplasia ratios increased with the diameters. A follow-up endoscopic examination of the 34 biopsied patients found the rate of complete resection by biopsy to be 79%. The largest lesion in which complete resection was expected was a low-grade dysplasia of 1.9 mm in diameter.

CONCLUSION: Minute pharyngeal lesions suspected to be dysplasia that are identified by NBI magnifying

endoscopy should be biopsied to determine the diagnosis and further treatment.

Key words: Biopsy; Minute pharyngeal lesions; Narrow-band imaging

Peer reviewers: Hoon Jai Chun, MD, PhD, AGAF, Professor, Department of Internal Medicine, Institute of Digestive Disease and Nutrition, Korea University College of Medicine, 126-1, Anam-dong 5-ga, Seongbuk-gu, Seoul 136-705, South Korea; Hiroki Nakamura, MD, Department of Gastroenterology and Hepatology, 1-1-1, Minami Kogushi, Ube, Yamaguchi 755-8505, Japan

Kumamoto T, Sentani K, Oka S, Tanaka S, Yasui W. Clinicopathological features of minute pharyngeal lesions diagnosed by narrow-band imaging endoscopy and biopsy. *World J Gastroenterol* 2012; 18(44): 6468-6474 Available from: URL: http://www.wjgnet.com/1007-9327/full/v18/i44/6468.htm DOI: http://dx.doi.org/10.3748/wjg.v18.i44.6468

INTRODUCTION

Magnified narrow-band imaging (NBI) endoscopy is reportedly useful for early pharyngeal[1-5] and esophageal cancer diagnosis[6-10]. Magnified NBI is useful both for detecting suspicious changes and for further diagnostic purposes, such as determining whether a lesion is suspected of being dysplasia or cancer[11,12]. We routinely examined upper gastrointestinal tracts using magnified NBI for one and a half years. When the unmagnified NBI detected a brownish area in the pharynx, a magnified NBI examination was used to aid the intrapapillary capillary loop (IPCL) classification[12-14]. If IPCL type Ⅳ or Ⅴ was observed, dysplasia or cancer was suspected, and treatment was considered. Although endoscopic submucosal dissection (ESD) leads to complete resection, ESD is an inpatient procedure that requires intubation anesthesia. For smaller (approximately 1 mm) lesions, therefore, our first choice is to biopsy the lesion for histological diagnosis while performing a complete resection. There have been no previous reports on the utility of biopsying minute pharyngeal lesions. This article reports our histological diagnosis, treatment, and follow-up findings from minute pharyngeal dysplasia biopsies.

MATERIALS AND METHODS

Patients

Most patients over 30 years old who require gastrointestinal endoscopy at the clinic are examined by magnified NBI. From August 2008 to March 2010, a total of 93 consecutive patients with IPCL type Ⅳ pharyngeal lesions, as determined by magnified NBI, were enrolled in this study (Table 1). The patients included 80 men aged 39-87 years (mean age, 66.9 years) and 13 women aged 43-84 years (mean age, 67.1 years). Drinking and smoking habits were assessed for 86 patients. Lesions of approximately 1 mm in diameter were found in 62 patients and were biopsied at the clinic, and the 17 patients with larger lesions were endoscopically resected by ESD at the Hiroshima University Hospital. Detailed histological assessments were performed for 62 of the biopsies. Thirty-four of the 62 biopsied patients received follow up endoscopy.

Instruments

The following instruments were used in this study: a magnifying endoscope that was capable of × 80 magnification (GIF H260Z; Olympus Optical Co. Ltd, Tokyo, Japan), a standard videoendoscopy system (EVIS LUCERA; Olympus), and an NBI system (Olympus).

Endoscopic examination

All of the endoscopic examinations were performed by the first author (Kumamoto T). A magnification hood (MB-46, Olympus) was attached to the tip of the endoscope. Intravenous access and pulse oximetry monitoring were established prior to the examination. Most of the examinations were performed under intravenous pethidine hydrochloride (17.5-70 mg) and midazolam (0.5-4 mg) sedation. The pharynx was mainly observed by NBI from the beginning of the examination. The pharynx was examined in the following order: uvula, posterior oropharyngeal wall, epiglottis, posterior hypopharyngeal wall, and pyriform sinus. The pharynx observation time was approximately 1 min. Magnified NBI was used for all pharynx lesions with noticeable brownish areas in the NBI examination, and an IPCL classification was performed. The IPCL classification followed the criteria of Dr. Inoue H[12,13]. According to these criteria, a lesion must meet three of the following four characteristics to be classified as IPCL type Ⅳ: dilatation, tortuous running, caliber changes, and different shapes in each IPCL[12-14]. In the 93 IPCL type Ⅳ lesions, smaller lesions of approximately 1 mm in diameter were biopsied with disposable biopsy forceps (FB-210K, Olympus). To avoid post-biopsy bleeding, all anticoagulants were discontinued from 3 d before to 3 d after the biopsy. The biopsy patients remained in the clinic for 2-3 h, including a 1 h post-sedation recovery time. Annual magnified NBI examinations were recommended to all of the biopsy patients, and 34 of 62 biopsy patients received follow up. To reduce inter-observer variation, the results of the NBI and magnified NBI examinations were independently evaluated by 2 endoscopy examiners (Kumamoto T and Oka S). When the evaluations differed, a consensus decision was achieved by reviewing the magnified NBI images.

Histological methods and criteria for pathological diagnosis

The biopsy specimens were extended and fixed to a styrene foam plate by fine acupuncture needles. All of the specimens were fixed in 10% formalin and embedded in

Table 1 Patient characteristics (n = 93)

Characteristics	No.
Age, yr (range)	67 (39-87)
Sex, men/women	80/13
Alcohol consumption	
Yes	56 (54 men, 2 women)
No	30 (22 men, 8 women)
Smoker	
Yes	57 (56 men, 1 woman)
No	29 (20 men, 9 women)
Esophageal cancer history	
Yes	2
No	91
Other cancer history	
Yes	9 (8 gastric cancer, 1 colon cancer)
No	84
Location	
Hypopharynx	21 (17 men, 4 women)
Oropharynx	72 (63 men, 9 women)
Biopsy cases	62
High-grade dysplasia	3
Low-grade dysplasia	25
Non-dysplasia	34
ESD cases	17
High-grade dysplasia	2
Low-grade dysplasia	14
Non-dysplasia	1

ESD: Endoscopic submucosal dissection.

Table 2 Histological characteristics of the biopsied pharyngeal lesions n (%)

	Non-D	LGD	HGD
Number	34	25	3
IPCL			
Upward extension	26 (76)	24 (96)	3 (100)
Dilatation and branching	5 (15)	21 (84)	3 (100)
Diameter expansion	0 (0)	8 (25)	1 (33)
Architectural atypia			
Proliferative cell distribution			
≥ 2/3	0 (0)	0 (0)	3 (100)
< 2/3	34 (100)	25 (100)	0 (0)
Tumor front	0 (0)	23 (92)	3 (100)
Cytological atypia			
Abnormal variation in cell size	0 (0)	2 (8)	3 (100)
Abnormal nuclear arrangement	0 (0)	23 (92)	3 (100)
Increased nuclear size			
High	0 (0)	0 (0)	3 (100)
Absent or low	34 (100)	25 (100)	0 (0)

Non-D: Non-dysplastic; LGD: Low-grade dysplasia; HGD: High-grade dysplasia; IPCL: Intra-papillary capillary loop.

paraffin wax. The tissue specimens were cut into 3-μm thick sections, and all of the sections received routine pathological diagnoses. The pathological parameters of each lesion were independently evaluated by two pathologists (Sentani K, Yasui W) and used for further analyses. The dysplasia diagnoses followed the criteria proposed by the World Health Organization[15]. In this study, dysplasia was classified as low-grade (mild or moderate dysplasia) or high-grade (severe dysplasia). These criteria were based on the architectural and cytological abnormalities. In addition to these abnormalities, IPCL changes were considered[16]. As shown in Table 2, the histological diagnoses were based on the IPCL changes and on architectural and cytological atypia. The IPCL changes were defined as upward extension, dilatation and branching, and diameter expansion. Architectural atypia was determined by a proliferative cell distribution and the tumor front, and cytological atypia was assessed by cell size, nuclear arrangement and nuclear size. The lesion diameters were measured under light microscopy using the built-in measurement system of the light microscope, which measured to an accuracy of 0.1 mm.

RESULTS

Minute pharyngeal lesions were diagnosed in 93 of approximately 3000 patients who were examined by magnified NBI. The clinicopathological characteristics of the patients are shown in Table 1. Of the 93 patients, 80 were men, and 13 were women. Fifty-six patients were drinkers, 57 were smokers, and 2 had esophageal cancer. Other cancers included gastric cancer in 8 patients and colon cancer in 1 patient. Twenty-one lesions were located on the posterior hypopharyngeal wall, and 72 lesions were found on the posterior oropharyngeal wall.

All 93 lesions were flat and showed similar findings in the magnified and unmagnified NBI examinations (Figures 1B, C; 2A, B). Most of the IPCL type Ⅳ lesions were identifiable immediately after the magnified NBI diagnosis by a faint redness under white light (Figure 1A). However, it was difficult to diagnose IPCL type Ⅳ lesions by this characteristic before an NBI examination because the contrast is weaker than that of NBI (Figure 1A, B). Of the 93 lesions, only 3 were greater than 2.1 mm in diameter, and the remaining lesions were less than 2.0 mm in diameter. Sixty-two lesions of approximately 1 mm in diameter were biopsied for histological diagnoses at the clinic, and 17 larger lesions were treated by ESD at the Hiroshima University Hospital. There were no complications, such as bleeding or pharyngeal pain, during or after the ESD.

The histological diagnoses of the 79 lesions resected by biopsy or ESD included 5 cases of high-grade dysplasia, 39 cases of low-grade dysplasia, and 35 non-dysplastic lesions. The 35 non-dysplastic cases consisted of 19 inflamed (pharyngitis) and 16 normal lesions. A lesion diagnosed as high-grade dysplasia is shown in Figure 1, and an example of low-grade dysplasia is shown in Figure 2. There were no cancerous lesions. The histological features of each type of dysplasia are shown in Table 2. In high-grade dysplasia, the polarity of the nucleus was lost, and the nuclear density was markedly increased throughout the intraepithelial layer, although the superficial portion of the epithelium was mature (Figure 1E). The microvascular irregularities were more severe than those seen in low-grade dysplasia. Basal cell palisading was observed in the low-grade dysplasia lesions; however, proliferative cells with enlarged nuclei that proliferated

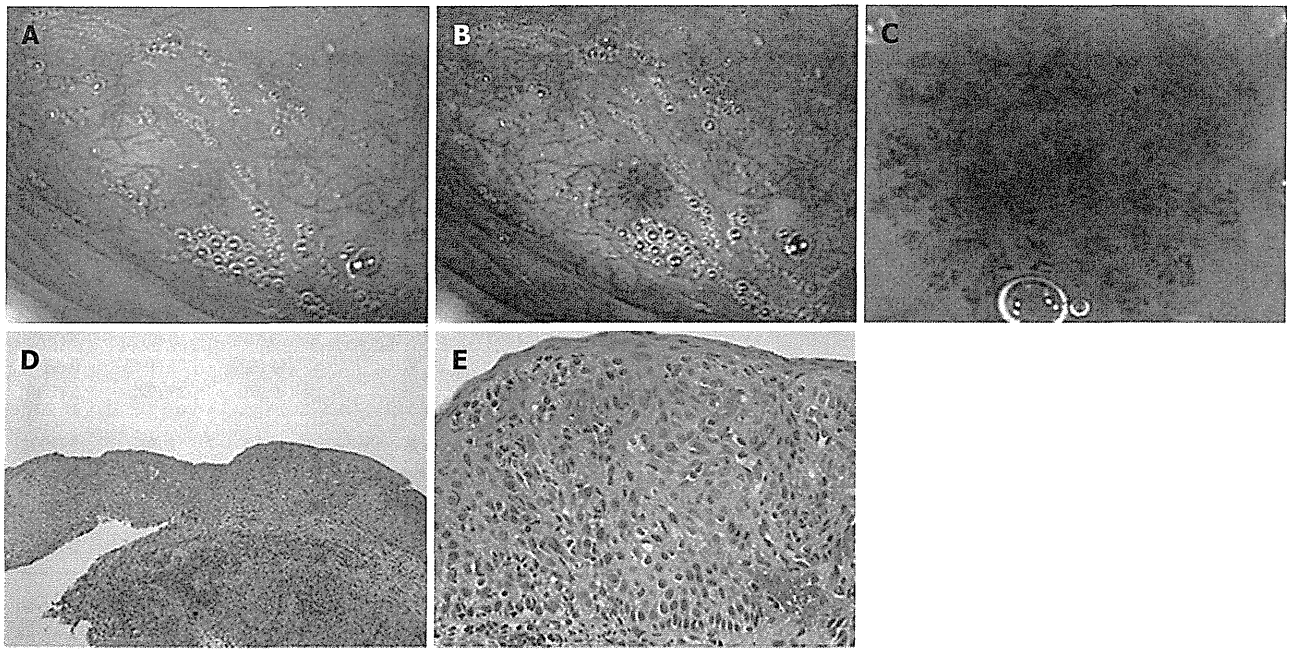

Figure 1 Narrow-band imaging view and histological image of high-grade dysplasia. A: An endoscopic photograph showing an oropharynx with high-grade dysplasia. The slightly reddish colored mucosa is the dysplastic lesion; B: The narrow-band imaging (NBI) corresponding to A, showing a well-demarcated brownish area; C: The magnified NBI view, showing an intra-papillary capillary loop type Ⅳ pattern. Irregular morphological changes in the superficial microvessels can be observed in the brownish area; D: Low-power magnification of the biopsied specimen, showing tumor front formation and complete epithelial layer invasion. The diameter of the lesion was 1.1 mm [hematoxylin and eosin (HE), original × 100]; E: Histologically, the lesion showed abnormal cell size variation and increased nuclear size; it was diagnosed as high-grade dysplasia (HE, original × 400).

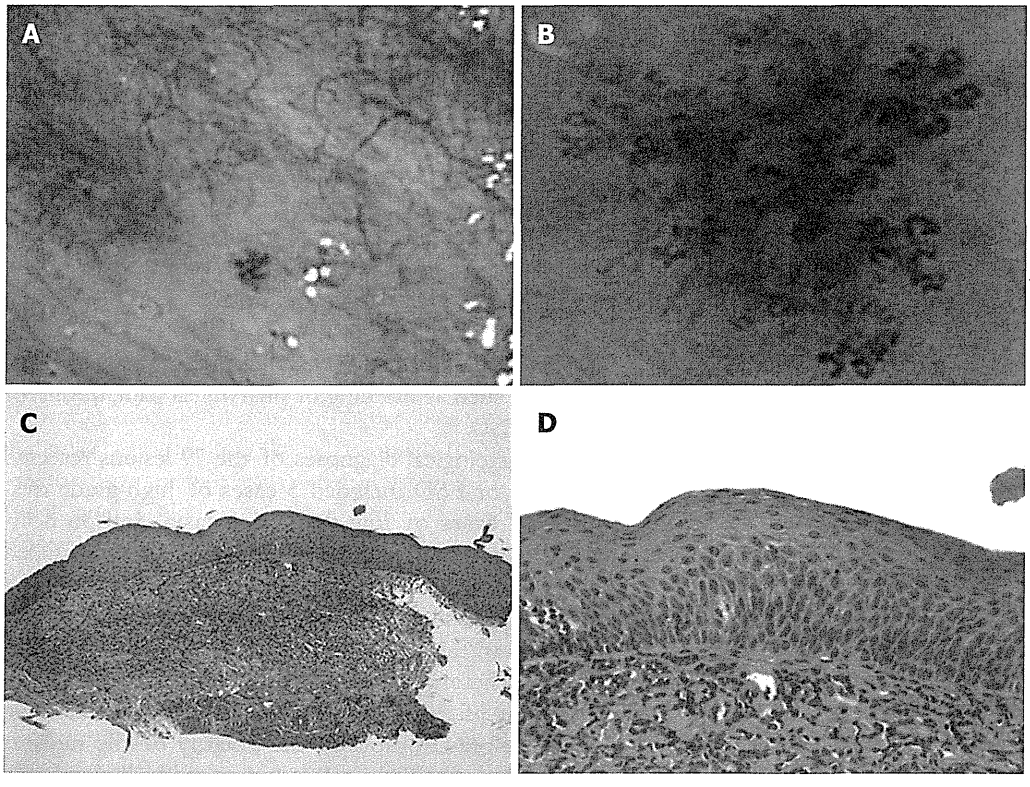

Figure 2 Narrow-band imaging view and histological image of low-grade dysplasia. A: Narrow-band imaging (NBI) showing the oropharynx with a well-demarcated brownish area; B: A magnified NBI magnifying view showing an intra-papillary capillary loop type Ⅳ pattern; C: Low power magnification of the biopsied specimen [hematoxylin and eosin (HE), original ×100]; D: Histologically, the lesion showed minimal cell size variation and was diagnosed as low-grade dysplasia (HE, original × 400).

Table 3 Diameters of the biopsied lesions *n* (%)

Diameter (mm)	*n*	Non-D	LGD	HGD
0.1-0.2	3	3 (100)	0 (0)	0 (0)
0.3-0.4	5	3 (60)	2 (40)	0 (0)
0.5-0.6	5	4 (80)	1 (20)	0 (0)
0.7-0.8	10	6 (60)	4 (40)	0 (0)
0.9-1.0	7	2 (29)	4 (57)	1 (14)
1.1-1.2	9	1 (11)	7 (78)	1 (11)
1.3-1.4	2	0 (0)	1 (50)	1 (50)
1.5-1.8	1	0 (0)	1 (100)	0 (0)
1.9-2.0	3	0 (0)	3 (100)	0 (0)

Non-D: Non-dysplasia; LGD: Low-grade dysplasia; HGD: High-grade dysplasia.

in a lamellar pattern were limited to the lower two-thirds of the epithelial layer (Figure 2D). IPCL abnormalities such as upward extension, dilatation, and diameter expansion were clearly recognized. In the high-grade dysplasia lesions, abnormal variations in cell size and increased nuclear size were observed in all of the lesions, whereas the incidence of these findings in the low-grade dysplasia lesions was low (Figures 1E, 2D). In the non-dysplastic lesions, such as inflamed squamous epithelium, intercellular edema and intraepithelial inflammatory cells were recognizable.

Of the 62 biopsied lesions, 45 were measurable (Table 3). The measured diameters were 0.1-2.0 mm (average, 1.12 mm); 30 lesions were 0.1-1.0 mm in diameter, and 15 lesions were 1.1-2.0 mm in diameter. The distribution of the lesion diameters and the neoplasia ratios are shown in Table 3. The dysplasia ratios (low-grade or high-grade) were 0% less than 0.2 mm, 20%-40% from 0.3 to 0.8 mm, 71% from 0.9 to 1.0 mm, 89% from 1.1 to 1.2 mm, and 100% from 1.3 to 2.0 mm. The ratio increased as the diameter increased. The diameters of the 3 high-grade lesions were 1.0, 1.1, and 1.3 mm.

Twenty-seven of the 34 biopsy patients who received endoscopic follow up (79%) had no lesions at the biopsy site in their NBI examinations, and complete resection from the biopsy was expected in these patients. The interval from the first diagnosis to the follow-up ranged from 4-22 mo (mean, 12.5 mo). The diameters of the lesions in the 3 incomplete resection cases were 0.7 mm, 1.1 mm, and 1.1 mm. Sixteen of the 34 cases were of high- or low-grade dysplasia, and 13 of these 16 cases (81%) had no lesions at the biopsy site. Complete resection from the biopsy was expected in these cases. The largest lesion for which complete resection was expected was 1.9 mm in diameter and was classified as low-grade dysplasia.

DISCUSSION

Magnified NBI endoscopy is preferable for diagnosing minute pharyngeal lesions[17-21]. The current practice at our clinic is to observe the pharynx and esophagus by NBI from the beginning of the examination. A distal magnification attachment on the endoscope tip is effective for quick focusing. The typical time for a magnified NBI examination from the pharynx to the duodenum was 10-15 min. The routine pharynx examination time was approximately 1 min.

During the period from September 2008 to March 2010, 93 patients with minute pharyngeal IPCL type Ⅳ lesions of approximately 1 mm in diameter were diagnosed at our clinic by magnified NBI endoscopy. During this period, we performed approximately 3000 routine examinations of the upper gastrointestinal tract using magnified NBI endoscopy. Thus, the frequency of such lesions was approximately 3%. Although it is well known that male drinkers and smokers aged over 50 are at high risk for pharyngeal carcinoma[22], we also observed several cases of low-grade dysplasia in women, and the youngest case was a 39-year-old man. Therefore, we routinely examine almost all men and women over 30 with magnified NBI endoscopy. In the present study, 2 patients had esophageal cancer[23-26], 8 had gastric cancer, and one had colon cancer. A history of other cancers may also be considered a risk factor.

All 93 lesions were intraepithelial flat lesions. Because the magnified NBI endoscopy findings were similar and showed no clear differences among high-grade dysplasia, low-grade dysplasia and non-dysplastic lesions, the 93 lesions appeared to have similar characteristics. If the lesions had been followed for a longer period, transitions from low-grade to high-grade dysplasia might have occurred. There is controversy over whether such lesions should be followed, biopsied, or treated. Because the histological diagnosis for 3 biopsied cases and 2 ESD cases was high-grade dysplasia, at least 5 lesions (all of which were in men) were considered to be precancerous. Although there were no cancerous lesions in this series[18], routinely using magnified NBI endoscopy seemed effective for diagnosing pharyngeal precancerous lesions early and showed that IPCL type Ⅳ lesions should be biopsied or resected by ESD. Because esophageal IPCL type Ⅳ lesions are thought to represent high-grade dysplasia, treatment is recommended[13]. However, treating smaller esophageal or pharyngeal IPCL type Ⅳ lesions (approximately 1 mm in diameter) is still controversial. Whether they should be treated or followed remains to be determined. Because the smaller pharyngeal IPCL type Ⅳ lesions in our study contained some precancerous lesions, we recommend biopsy and treatment over follow up.

A survey of the diameters of the biopsied lesions indicated an increase in the dysplasia ratio as the diameter increased, and all lesions over 1.3 mm were found to be dysplastic. Our clinic sees typical outpatients with varied gastrointestinal symptoms or abnormal gastric X-ray findings, and the diameter distribution we observed appears to be close to the natural distribution of such lesions. The diameter of the 3 high-grade lesions ranged from 1.0 to 1.3 mm; therefore, it would appear that lesions greater than 1.0 mm in diameter should be resected by biopsy or ESD. Furthermore, because low-grade lesions as small as 0.3 mm in diameter were observed, it would be better to

resect all lesions less than 1.0 mm in diameter. The diameter distribution appears to show the natural progression from low-grade to high-grade dysplasia.

A follow-up study of the biopsied cases revealed that the resection rate by biopsy alone was 79%. The diameter of the largest resected lesion was 1.9 mm. Although annual endoscopic follow-up must be continued, biopsy may lead to complete resection in some cases and can be performed as a first-line therapy. Single-use disposable biopsy forceps were used to obtain a biopsy specimen as large and as deep as possible for complete resection. For the biopsy, the plane of the opened biopsy forceps should be horizontal, which can be achieved by rotating the handle. Precise, lesion-centered biopsies of 1 mm lesions are difficult[13] and require high levels of concentration and cooperation between the examiner and the assisting medical staff. Recently, we have biopsied these lesions prior to inserting the endoscope into the esophagus because if we try to biopsy during the final withdrawal stage, the observations may be disturbed by secreted mucus and minute bleeding. Biopsying the pharynx appeared to be safe providing all anticoagulant drugs were discontinued from 3 d before to 3 d after biopsy. We experienced no complications (such as bleeding) after the biopsies.

Compared to the esophagus, the pharynx is sensitive to being touched by an endoscope. Therefore, almost all of the magnified NBI magnifying examinations were performed under sedation. The hypopharynx is particularly sensitive. Without sedation, the pharyngeal reflex causes responsive artificial bleeding, particularly when touched by the distal attachment during examination, and NBI observation becomes difficult due to the brownish color change in the entire endoscopic field. In our experience, magnified NBI endoscopy can be routinely performed with the patient under sedation. However, because deep sedation may cause respiratory depression, sedation should be used cautiously with an intravenous drip, and with oxygen and the counteracting effect of flumazenil readily available. In high-risk patients, such as those with respiratory or heart disease, for safety, we removed the distal attachment on the scope tip or changed the scope to a smaller diameter non-magnifying scope (GIF H260, Olympus).

In conclusion, magnified NBI endoscopy appears to be preferable for diagnosing pharyngeal neoplasia. Biopsy was useful for the diagnosis and treatment of minute pharyngeal neoplasia.

COMMENTS

Background

It has been difficult to diagnose an early-stage pharyngeal carcinoma. Narrow-band imaging (NBI) has enabled more accurate diagnosis and increased the detection rate of superficial pharyngeal carcinomas. Magnified NBI endoscopy is quite effective for diagnosing early-stage pharyngeal and esophageal carcinoma, that is, carcinomas in the squamous cell regions. The intrapapillary capillary loop (IPCL) classification for magnified NBI endoscopy is applicable only to the squamous cell regions, that is, the pharynx and the esophagus. Magnified NBI endoscopy for the stomach and the colon is evaluated by different diagnostic classifications.

Research frontiers

Magnified NBI endoscopy made it possible to diagnose minute pharyngeal lesions with diameters of approximately 1 mm. It includes two steps. First, using NBI endoscopy without magnification, the authors detected suspicious changes as brownish areas. Second, using NBI magnifying of the brownish areas, the authors were able to diagnose whether the changes were suspicious of dysplasia or cancer or not according to the IPCL classification. IPCL type Ⅳ or Ⅴ shows the possibility of dysplasia or cancer, whereas IPCL type Ⅰ neglects the possibility.

Innovations and breakthroughs

For larger pharyngeal IPCL type Ⅳ lesions over 10 mm diameter, endoscopic submucosal dissection (ESD) is recommended. However, for smaller lesions of approximately 1 mm diameter, it remains to be determined whether they should be resected by ESD or followed up. Studies on the biopsy of such lesions are few. The authors concluded that biopsy can be the first-line procedure for such lesions not only for diagnosis but also for treatment.

Applications

The NBI system and magnifying endoscope are necessary to begin magnified NBI endoscopy. As the pharynx is sensitive, magnified NBI endoscopy of the pharynx should be performed under sedation. For safety, sedation should be carried out cautiously. As several biopsied minute pharyngeal lesions were high grade dysplasia, minute pharyngeal lesions should be biopsied for diagnosis. Furthermore, follow-up study of the biopsied lesions showed that even complete resection was expected by biopsy.

Terminology

NBI: NBI is a new image-enhanced optical technology that uses narrow band NBI filters; IPCL: IPCL is the microvascular tumor vessel classification system used for NBI magnifying endoscopy.

Peer review

Recently it has been reported that NBI can be useful in the early detection of superficial pharyngeal cancer. To determine the criteria of endoscopic treatment in patients with pharyngeal cancer and dysplasia, the resected specimen and follow up data are required. It is a good idea to investigate the usefulness of NBI magnifying endoscopy in the pharynx because biopsy in the pharynx is difficult.

REFERENCES

1 **Nonaka S**, Saito Y. Endoscopic diagnosis of pharyngeal carcinoma by NBI. *Endoscopy* 2008; **40**: 347-351

2 **Muto M**, Nakane M, Katada C, Sano Y, Ohtsu A, Esumi H, Ebihara S, Yoshida S. Squamous cell carcinoma in situ at oropharyngeal and hypopharyngeal mucosal sites. *Cancer* 2004; **101**: 1375-1381

3 **Ugumori T**, Muto M, Hayashi R, Hayashi T, Kishimoto S. Prospective study of early detection of pharyngeal superficial carcinoma with the narrowband imaging laryngoscope. *Head Neck* 2009; **31**: 189-194

4 **Watanabe A**, Tsujie H, Taniguchi M, Hosokawa M, Fujita M, Sasaki S. Laryngoscopic detection of pharyngeal carcinoma in situ with narrowband imaging. *Laryngoscope* 2006; **116**: 650-654

5 **Matsuba H**, Katada C, Masaki T, Nakayama M, Okamoto T, Hanaoka N, Tanabe S, Koizumi W, Okamoto M, Muto M. Diagnosis of the extent of advanced oropharyngeal and hypopharyngeal cancers by narrow band imaging with magnifying endoscopy. *Laryngoscope* 2011; **121**: 753-759

6 **Yoshida T**, Inoue H, Usui S, Satodate H, Fukami N, Kudo SE. Narrow-band imaging system with magnifying endoscopy for superficial esophageal lesions. *Gastrointest Endosc* 2004; **59**: 288-295

7 **Muto M**, Minashi K, Yano T, Saito Y, Oda I, Nonaka S, Omori T, Sugiura H, Goda K, Kaise M, Inoue H, Ishikawa H, Ochiai A, Shimoda T, Watanabe H, Tajiri H, Saito D. Early detection of superficial squamous cell carcinoma in the head and neck region and esophagus by narrow band imaging: a multicenter randomized controlled trial. *J Clin Oncol* 2010;

28: 1566-1572

8 **Muto M**, Hironaka S, Nakane M, Boku N, Ohtsu A, Yoshida S. Association of multiple Lugol-voiding lesions with synchronous and metachronous esophageal squamous cell carcinoma in patients with head and neck cancer. *Gastrointest Endosc* 2002; **56**: 517-521

9 **Muto M**, Takahashi M, Ohtsu A, Ebihara S, Yoshida S, Esumi H. Risk of multiple squamous cell carcinomas both in the esophagus and the head and neck region. *Carcinogenesis* 2005; **26**: 1008-1012

10 **Muto M**, Katada C, Sano Y, Yoshida S. Narrow band imaging: a new diagnostic approach to visualize angiogenesis in superficial neoplasia. *Clin Gastroenterol Hepatol* 2005; **3**: S16-S20

11 **Muto M**, Ugumori T, Sano Y, Ohtsu A. Yoshida S. Narrow-band imaging combined with magnified endoscopy for cancer at the head and neck region. *Dig Endosc* 2005; **17**: S23-S24

12 **Inoue H**. Magnification endoscopy in the esophagus and stomach. *Dig Endosc* 2001; **13**: S40-S41

13 **Inoue H**, Kaga M, Sato Y, Sugaya S, Kudo S. Magnifying endoscopic diagnosis of tissue atypia and cancer invasion depth in the area of pharyngo-esophageal squamous epithelium by NBI enhanced magnification image: IPCL pattern classification. In: Cohen J. Advanced Digestive Endoscopy: Comprehensive Atlas of High Resolution Endoscopy and Narrowband Imaging. Oxford: Wiley-Blackwell, 2007:49-66

14 **Kumagai Y**, Inoue H, Nagai K, Kawano T, Iwai T. Magnifying endoscopy, stereoscopic microscopy, and the microvascular architecture of superficial esophageal carcinoma. *Endoscopy* 2002; **34**: 369-375

15 **Barnes L**, Eveson JW, Reichart P, Sidransky D (Eds): World Health Organization Classification of Tumours. Pathology and Genetics of Head and Neck Tumours. Lyon: IARC Press, 2005

16 **Fujii S**, Yamazaki M, Muto M, Ochiai A. Microvascular irregularities are associated with composition of squamous epithelial lesions and correlate with subepithelial invasion of superficial-type pharyngeal squamous cell carcinoma. *Histopathology* 2010; **56**: 510-522

17 **Yoshimura N**, Goda K, Tajiri H, Yoshida Y, Kato T, Seino Y, Ikegami M, Urashima M. Diagnostic utility of narrow-band imaging endoscopy for pharyngeal superficial carcinoma. *World J Gastroenterol* 2011; **17**: 4999-5006

18 **Tanaka S**, Morita Y, Fujita T, Yokozaki H, Obata D, Fujiwara S, Wakahara C, Masuda A, Sugimoto M, Sanuki T, Yoshida M, Toyonaga T, Kutsumi H, Azuma T. Clinicopathological characteristics of abnormal micro-lesions at the oro-hypopharynx detected by a magnifying narrow band imaging system. *Dig Endosc* 2012; **24**: 100-109

19 **Shimizu Y**, Tsukagoshi H, Fujita M, Hosokawa M, Watanabe A, Kawabori S, Kato M, Sugiyama T, Asaka M. Head and neck cancer arising after endoscopic mucosal resection for squamous cell carcinoma of the esophagus. *Endoscopy* 2003; **35**: 322-326

20 **Katada C**, Nakayama M, Tanabe S, Koizumi W, Masaki T, Takeda M, Okamoto M, Saigenji K. Narrow band imaging for detecting metachronous superficial oropharyngeal and hypopharyngeal squamous cell carcinomas after chemoradiotherapy for head and neck cancers. *Laryngoscope* 2008; **118**: 1787-1790

21 **Katada C**, Tanabe S, Koizumi W, Higuchi K, Sasaki T, Azuma M, Katada N, Masaki T, Nakayama M, Okamoto M, Muto M. Narrow band imaging for detecting superficial squamous cell carcinoma of the head and neck in patients with esophageal squamous cell carcinoma. *Endoscopy* 2010; **42**: 185-190

22 **Yokoyama A**, Kato H, Yokoyama T, Tsujinaka T, Muto M, Omori T, Haneda T, Kumagai Y, Igaki H, Yokoyama M, Watanabe H, Fukuda H, Yoshimizu H. Genetic polymorphisms of alcohol and aldehyde dehydrogenases and glutathione S-transferase M1 and drinking, smoking, and diet in Japanese men with esophageal squamous cell carcinoma. *Carcinogenesis* 2002; **23**: 1851-1859

23 **Morita M**, Kuwano H, Ohno S, Sugimachi K, Seo Y, Tomoda H, Furusawa M, Nakashima T. Multiple occurrence of carcinoma in the upper aerodigestive tract associated with esophageal cancer: reference to smoking, drinking and family history. *Int J Cancer* 1994; **58**: 207-210

24 **Nonaka S**, Saito Y, Oda I, Kozu T, Saito D. Narrow-band imaging endoscopy with magnification is useful for detecting metachronous superficial pharyngeal cancer in patients with esophageal squamous cell carcinoma. *J Gastroenterol Hepatol* 2010; **25**: 264-269

25 **Matsubara T**, Yamada K, Nakagawa A. Risk of second primary malignancy after esophagectomy for squamous cell carcinoma of the thoracic esophagus. *J Clin Oncol* 2003; **21**: 4336-4341

26 **Piazza C**, Cocco D, De Benedetto L, Bon FD, Nicolai P, Peretti G. Role of narrow-band imaging and high-definition television in the surveillance of head and neck squamous cell cancer after chemo- and/or radiotherapy. *Eur Arch Otorhinolaryngol* 2010; **267**: 1423-1428

S- Editor Lv S **L- Editor** Webster JR **E- Editor** Zhang DN

IJC
International Journal of Cancer

Stroma-directed imatinib therapy impairs the tumor-promoting effect of bone marrow-derived mesenchymal stem cells in an orthotopic transplantation model of colon cancer

Kei Shinagawa[1], Yasuhiko Kitadai[1], Miwako Tanaka[1], Tomonori Sumida[1], Mieko Onoyama[1], Mayu Ohnishi[1], Eiji Ohara[1], Yukihito Higashi[2], Shinji Tanaka[3], Wataru Yasui[4] and Kazuaki Chayama[1]

[1] Department of Gastroenterology and Metabolism, Graduate School of Biomedical Sciences, Hiroshima University, Hiroshima, Japan
[2] Department of Cardiovascular Physiology and Medicine, Graduate School of Biomedical Sciences, Hiroshima University, Hiroshima, Japan
[3] Department of Endoscopy, Hiroshima University Hospital, Hiroshima, Japan
[4] Department of Molecular Pathology, Graduate School of Biomedical Sciences, Hiroshima University, Hiroshima, Japan

Bone marrow-derived mesenchymal stem cells (MSCs) are reported to contribute to formation of tumor-promoting stromal cells. We reported recently that, in an orthotopic nude mice model of colon cancer, MSCs traveled to tumor stroma, where they differentiated into carcinoma-associated fibroblast (CAF)-like cells. We also found that CAFs express platelet-derived growth factor receptor (PDGFR) at a high level and that imatinib therapy targeting PDGFR in CAFs inhibits growth and metastasis of human colon cancer. These findings led us to examine whether the tumor-promoting effect of MSCs is impaired by blockade of PDGFR signaling achieved with imatinib. Orthotopic transplantation and splenic injection of human MSCs along with KM12SM human colon cancer cells, in comparison with transplantation of KM12SM cells alone, resulted in significantly greater promotion of tumor growth and liver metastasis. The KM12SM + MSC xenograft enhanced cell proliferation and angiogenesis and inhibited tumor cell apoptosis. When tumor-bearing animals were treated with imatinib, there was no significant increase in primary tumor volume or total volume of liver metastases, despite the KM12SM+MSC xenograft, and survival in the mixed-cell group was prolonged by imatinib treatment. Moreover, the ability of MSCs to migrate to tumor stroma was impaired, and the number of MSCs surviving in the tumor microenvironment was significantly decreased. In *in vitro* experiments, treatment with imatinib inhibited migration of MSCs. Our data suggest that blockade of PDGF signaling pathways influences the interaction between bone marrow-derived MSCs and tumor cells in the tumor microenvironment and, hence, inhibits the progressive growth of colon cancer.

Cancer Cell Biology

Key words: mesenchymal stem cells, carcinoma-associated fibroblasts, orthotopic colon cancer model, platelet-derived growth factor receptor, imatinib

Abbreviations: CAF: carcinoma-associated fibroblast; DAPI: 4′,6-diamidino-2-phenylindole; DMEM: Dulbecco's Modified Eagle's Medium; FBS: fetal bovine serum; HBSS: Hanks' balanced salt solution; MSC: mesenchymal stem cell; MVA: microvessel area; PCNA: proliferating cell nuclear antigen; PCNA-LI: PCNA labeling index; PDGF: platelet-derived growth factor; PDGFR: platelet-derived growth factor receptor

Grant sponsors: Grants-in-Aid for Cancer Research from the Ministry of Education, Culture, Science, Sports and Technology of Japan, Ministry of Health, Labor and Welfare of Japan
DOI: 10.1002/ijc.27735
History: Received 12 Oct 2011; Accepted 28 Jun 2012; Online 23 Jul 2012

Correspondence to: Yasuhiko Kitadai, Department of Gastroenterology and Metabolism, Graduate School of Biomedical Sciences, Hiroshima University, 1-2-3 Kasumi, Minami-Ku, Hiroshima 734-8551, Japan, Tel.: +81-82-257-5191, Fax: +81-82-257-5194, E-mail: kitadai@hiroshima-u.ac.jp

Many recent reports have referred to tumor-stromal interactions as essential events for tumor progression.[1–3] Of the constituents of tumor stroma, it has become clear that activated fibroblasts, called carcinoma-associated fibroblasts (CAFs), promote tumor growth and metastasis.[4–8] We previously reported that the platelet-derived growth factor (PDGF)/PDGF receptor (PDGFR) signaling pathway plays a critical role in the growth and metastasis of gastric and colon cancers in orthotopic transplantation models.[4,8] Tumor cells express PDGFs, and PDGFRs are expressed by CAFs. The origin of CAFs is not fully understood, but they may arise from fibroblasts residing in local tissues,[7] periadventitial cells including pericytes and vascular smooth muscle cells,[9] endothelial cells,[10] and bone marrow-derived cells including various stem cells.[11]

Mesenchymal stem cells (MSCs) can be recruited from bone marrow to inflamed or damaged tissues by local endocrine signals, resulting in tissue regeneration.[12,13] Although MSCs are known to migrate to a variety of tumors, such as melanomas,[14] gliomas,[15,16] and colon,[17,18] pancreatic,[19,20] and breast cancers,[21–23] the mechanisms of the migratory effect are very complex, and the key factors have not been identified. Experimental co-injection of tumor cells and MSCs has revealed

What's new?

Platelet-derived growth factor (PDGF) signaling pathways are crucial for the migration of metastasis-promoting mesenchymal stem cells (MSCs) to the tumor microenvironment in human colon cancer. In this study employing orthotopic transplantation of human MSCs and colon cancer cells in mice, inhibition of PDGF signaling with the drug imatinib was found to influence interactions between bone marrow-derived MSCs and tumor cells, suggesting that stroma-directed imatinib therapy could be effective against colon cancer progression.

that MSCs promote tumor growth and metastasis[22,24–33] and are implicated in tumor invasion and angiogenesis,[17,24,30,31] immunosuppression,[25,26] inhibition of apoptosis,[29] and formation of a cancer stem cell niche.[32] Our recent study showed that MSCs accumulating in the tumor microenvironment differentiate into CAFs and promote growth and metastasis of colon cancer.[34] Very recently, it was shown in a mouse model of gastric cancer that at least 20% of CAFs originate from bone marrow-derived MSCs.[35] PDGF signaling pathways are known to be crucial to migration and survival of MSCs.[15,19,36]

In an orthotopic transplantation model of human colon cancer, we examined the effect of imatinib, known to be a potent tyrosine kinase inhibitor of PDGFR,[37] on migration and survival of MSCs in the tumor microenvironment and on promotion of tumor growth and metastasis by MSCs. We found that treatment with imatinib inhibited tumor-MSC interactions and modified tumor-supporting stroma.

Material and Methods

Cell culture

Human MSCs were harvested from the iliac crest and isolated and cultured according to a protocol approved by the Ethics Committee of Hiroshima University Graduate School of Medicine, as described previously.[34,38] The capacity for chondrogenic, adipogenic, and osteogenic differentiation was confirmed with the use of a Human Mesenchymal Stem Cell Functional Identification Kit (R&D Systems, Minneapolis, MN). Cell surface antigens on the MSCs were analyzed by fluorescence-activated cell sorting, and it was confirmed that the cells were positive for CD29, CD44, CD73, CD90, CD105, CD166, and MHC-DR but negative for CD14, CD34, and Flk-1, as described previously.[38] MSCs were fluorescently labeled with red fluorescent linker dye (PKH26 Red Fluorescent Cell Linker Kit; Sigma, Sigma-Aldrich, St Louis, MO) according to the manufacturer's instructions.

Human colon cancer cell line KM12SM[39] was kindly gifted by Dr. Isaiah J. Fidler (University of Texas). Cells were maintained in DMEM supplemented with 10% fetal bovine serum (FBS), L-glutamine, and a penicillin-streptomycin solution. The cultures were maintained for no longer than 12 weeks after recovery of cells from frozen stock.

Animals and transplantation of tumor cells

Female athymic BALB/c nude mice were obtained from Charles River Japan (Tokyo, Japan). The mice were maintained under specific pathogen-free conditions and used at 8 weeks of age. The study was carried out after permission was granted by the Committee on Animal Experimentation of Hiroshima University.

To produce cecal tumors, KM12SM cells in 50 μL of Hanks' balanced salt solution (HBSS) were injected into the cecal wall of nude mice under observation with a zoom stereomicroscope. To produce experimental liver metastases, the cells were injected into the spleen of nude mice as described previously.[39]

Anticancer drug

Imatinib (imatinib mesylate or Gleevec; Novartis Pharma AG, Basel, Switzerland) was diluted in sterile water for administration by oral gavage.

Effect of imatinib on tumor tropism of MSCs in vivo

Because we have found that MSCs migrate to orthotopic and metastatic tumor sites,[34] we examined whether imatinib affects the tumor tropism of MSCs. We injected 0.5×10^6 KM12SM cells into the cecal wall in six mice on day 0. One week after the orthotopic implantation of tumor cells (on day 7), mice were randomized into two groups: one given water daily (control group) and the other given 50 mg/kg/day imatinib by oral gavage once daily until day 28. Three weeks after tumor cell transplantation (on day 21), each mouse was injected with 1.0×10^6 PKH26-labeled MSCs (in 200 μL of HBSS) in the tail vein. One week after this injection (on day 28), the mice were killed and necropsied.

KM12SM cells (0.5×10^6) were transplanted into the spleen of six additional mice on day 0. One week after tumor cell transplantation (on day 7), mice were randomized into two groups: one given water daily (control group) and the other given 50 mg/kg/day imatinib by oral gavage once daily until day 28. At the same time (on day 7), each mouse was injected with 1.0×10^6 PKH26-labeled MSCs (in 200 μL of HBSS) in the tail vein. Three weeks after this injection (on day 28), the mice were killed.

Necropsy procedures and histologic studies

Mice bearing orthotopic tumors were killed with an overdose of methophane. Necropsy was performed, after which tumors were excised and measured. For immunohistochemical and hematoxylin and eosin (H&E) staining, one part of the tumor tissue was fixed in formalin-free IHC Zinc Fixative (PharMingen, San Diego, CA) and embedded in paraffin, and the

other part was embedded in OCT compound (Sakura Finetek Japan, Tokyo, Japan), rapidly frozen in liquid nitrogen, and stored at −80°C. Sections of PKH26-labeled tissues were analyzed by means of fluorescence confocal microscopy.

Effect of imatinib on interactions between tumor cells and MSCs in orthotopic colon tumor

To examine the effect of imatinib on the tumor-MSC interactions in orthotopic colon tumors, co-injection studies were carried out. Mice were divided into four groups according to the kind(s) of implanted cells and the treatment received: (*i*) KM12SM cells alone and daily administration of water by oral gavage (0.5×10^6, $n = 19$), (*ii*) KM12SM cells mixed with MSCs and daily administration of water by oral gavage (KM12SM:MSC ratio, 0.5×10^6:1.0×10^6 [1:2]; $n = 21$), (*iii*) KM12SM cells alone and daily oral gavage 50 mg/kg imatinib (0.5×10^6, $n = 8$), or (*iv*) KM12SM cells mixed with MSCs and daily oral gavage 50 mg/kg imatinib [KM12SM:MSC ratio, 0.5×10^6:1.0×10^6, [1:2]; $n = 12$).

Treatment with imatinib was begun 1 week after intracecal transplantation of cells and lasted 5 weeks. Surviving mice were then killed and necropsied [(*i*) $n = 18$, (*ii*) $n = 10$, (*iii*) $n = 8$, (*iv*) $n = 10$]. Tumor volume, incidence of liver metastasis, and survival were evaluated. Tumor volume (V) was calculated as $V = (1/2)ab^2$, where a is the largest diameter of the tumor and b is the smallest diameter.

Quantification of the remaining MSCs and phosphorylation of PDGFR-β in MSCs coimplanted with tumor cells in vivo

To evaluate how many MSCs coimplanted with tumor cells remained at the orthotopic tumor site, and whether PDGFR-β in MSCs was phosphorylated, KM12SM cells mixed with PKH26-labeled MSCs (0.5×10^6:1.0×10^6 [1:2]) were injected into the cecal wall in three mice. Three weeks after intracecal transplantation, tumors were excised and analyzed by means of fluorescence confocal microscopy to detect PKH26-labeled MSCs and to confirm phosphorylation of PDGFR-β in MSCs by immunofluorescence staining as described previously.[34] For quantification of the remaining MSCs, 10 random fields were captured with a 20× objective lens, and red fluorescence areas were measured. The areas were calculated with the use of NIH ImageJ software.

Effect of imatinib on interactions between tumor cells and MSCs in a liver metastasis model

To evaluate the effect of imatinib on the tumor-MSC interactions in liver metastases, we developed a model of liver metastasis by injecting tumor cells into mice spleen as described previously.[39] Mice were divided into four groups according to the kind(s) of implanted cells and the treatment received ($n = 10$ in each group): (*i*) KM12SM cells alone and daily administration of water by oral gavage (0.5×10^6), (*ii*) KM12SM cells mixed with PKH26-labeled MSCs and daily administration of water by oral gavage (KM12SM:PKH26-labeled MSC ratio, 0.5×10^6:1.0×10^6 [1:2]), (*iii*) KM12SM cells alone and daily oral gavage 50 mg/kg imatinib (0.5×10^6), (*iv*) KM12SM cells mixed with PKH26-labeled MSCs and daily oral gavage 50 mg/kg imatinib (KM12SM:PKH26-labeled MSCs, 0.5×10^6:1.0×10^6 [1:2]).

One week after intrasplenic transplantation of cells, mice were treated with imatinib for 3 weeks; surviving mice were then killed and necropsied ($n = 10$ in each group). Tumor nodules on the liver surface were counted macroscopically. Metastatic tumors were analyzed by means of fluorescence confocal microscopy to detect PKH26-labeled MSCs.

Antibodies

Rabbit anti-PDGFR-β and rabbit antiphosphorylated PDGFR-β (p-PDGFR-β) (Santa Cruz Biotechnology, Santa Cruz, CA), mouse antiproliferating cell nuclear antigen (PCNA) (Dako, Glostrup, Denmark), and rat anti-mouse CD31 (BD Pharmingen, San Diego, CA) were used as primary antibodies. Biotinylated rabbit anti-rat IgG (Dako) and biotinylated goat anti-mouse IgG (Dako) were used as secondary antibodies. Alexa Fluor® 488-labeled goat anti-rabbit IgG (Invitrogen, Carlsbad, CA) was used as fluorescent secondary antibody.

Immunohistochemical determination of PCNA, apoptotic cells, and microvessel area (MVA)

Paraffin-embedded tissues cut into 4 μm sections and frozen tissues cut into 8 μm sections were used for immunohistochemical identification of PCNA and CD31, respectively. Immunohistochemistry was performed as described previously.[40] The PCNA labeling index (PCNA-LI) was taken as the ratio of positively stained tumor cells to the total tumor cells and expressed as a percentage for each case.[34] Apoptotic cells in paraffin sections of KM12SM tumors were detected by terminal deoxynucleotide transferase-mediated dUTP-biotin nick end labeling with the ApopTag Plus Peroxidase In Situ Apoptosis Detection Kit (Chemicon, Temecula, CA) according to the manufacturer's instructions. The apoptotic index (AI) was taken as the ratio of positively stained tumor cells and apoptotic bodies to all tumor cells and expressed as a percentage for each case.[34] Angiogenic activity was evaluated according to the areas of microvessels stained with anti-mouse CD31 antibody. For quantification of the MVA, 10 random fields at 100× magnification were captured for each tumor, and the outline of each microvessel including a lumen was manually traced. The area was then calculated with the use of NIH ImageJ software.

Confocal microscopy

Confocal fluorescence images were captured with a 20× or 40× objective lens on a Zeiss LSM 510 laser scanning microscopy system (Carl Zeiss Inc., Thornwood, NY) equipped with a motorized Axioplan microscope, argon laser (458/477/488/514 nm, 30 mW), HeNe laser (543 nm, 1 mW), HeNe laser (633 nm, 5 mW), LSM 510 control and image acquisition software, and appropriate filters (Chroma Technology Corp., Brattleboro, VT). Confocal images were exported to Adobe Photoshop software, and image montages were prepared.

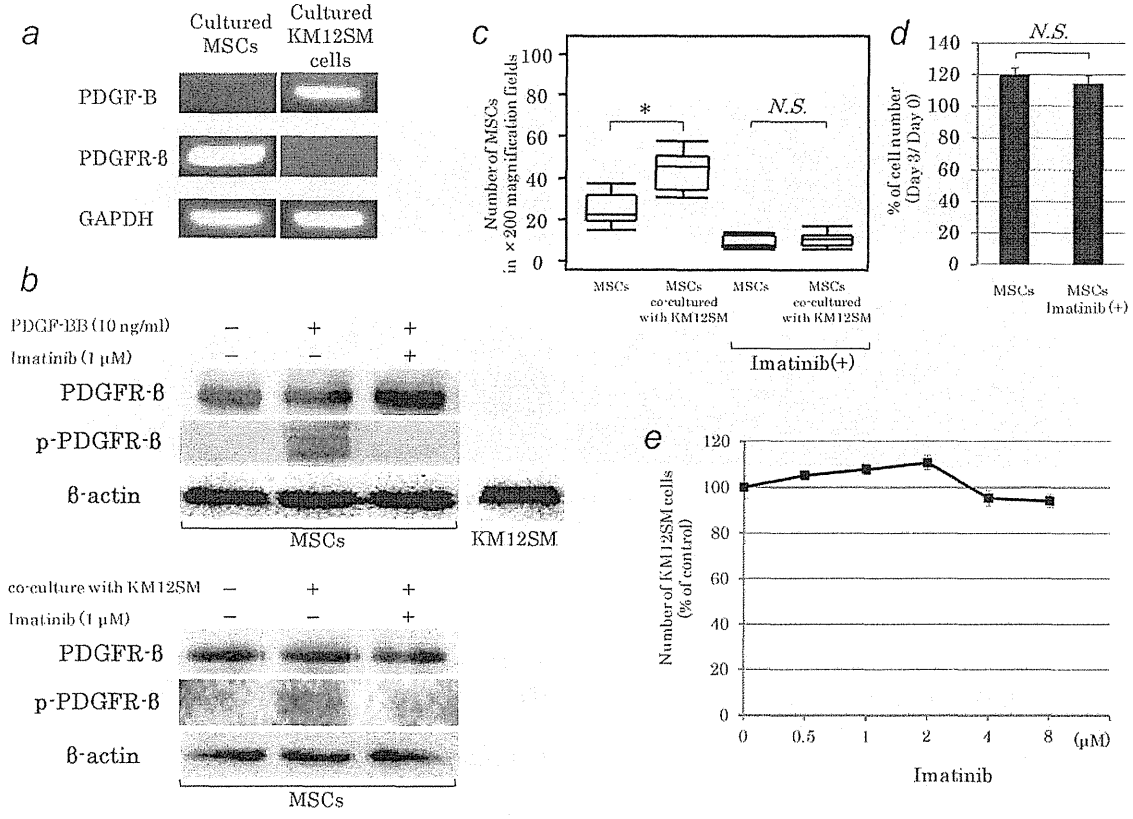

Figure 1. Effect of imatinib on KM12SM cells and MSCs *in vitro*. (*a*) Reverse transcription-polymerase chain reaction and (*b*) Western blot analyses for expression of PDGF-B and PDGFR-β in MSCs and KM12SM cells. PDGFR-beta in MSCs was phosphorylated by coculture with KM12SM cells. Phosphorylation of PDGFR-β in MSCs was inhibited by 1 μM imatinib. (*c*) Migratory ability of MSCs evaluated by transwell assay. The tumor tropism of MSCs was impaired by imatinib treatment, but 1 μM imatinib did not affect proliferation of MSCs (*d*). (*e*) Dose–response curve for imatinib and its growth inhibiting effect in KM12SM cells. *$p < 0.05$, bars: SE.

Migration assay

The migratory ability of MSCs was assayed with the use of a 24-well microchamber plate with uncoated inserts (8 μm pore size, Corning Costar, Tokyo, Japan). Either 2.0×10^4 KM12SM cells in DMEM with 0.5% FBS or medium alone was plated into the lower chambers. After 24 hr of incubation at 37°C, upper chambers containing 2.0×10^4 MSCs in DMEM with 0.5% FBS or 0.5% FBS and 1 μM imatinib, were set into the lower chambers. Three wells were used for each experiment. After 28 hr of incubation at 37°C, inserts were fixed with 10% buffered formalin solution and stained with hematoxylin. The cells on the upper surface of the membranes were removed with cotton swabs. The number of migrating cells was counted in three random fields per filter at 200× magnification.

Proliferation assay

The effect of imatinib on the proliferation of KM12SM cells was analyzed. KM12SM (4.0×10^5) cells were seeded in a 6-well plate in DMEM with 0.5% FBS and 0, 0.5, 2.0, 4.0, or 8.0 μM imatinib. The medium was changed every day, and the number of cells was counted on days 3 and 6 ($n = 6$ in each group).

In vitro growth of KM12SM cells was measured with a Cell Proliferation Biotrak ELISA System, version 2 (Amersham Biosciences, Piscataway, NJ), according to the manufacturer's instructions. Cells were seeded in a 96-well plate at a density of 0.5×10^4 cells/well and incubated overnight in 200 μL culture medium containing 10% FBS. After incubation for 24 hr, cells were cultured in serum-free culture medium containing 10 μM BrdU with or without imatinib for 24 hr, and cell proliferation was measured in a plate reader (Microplate Manager 5.2.1, BIO-RAD, Hercules, CA) at 450 nm.

Western blot analysis

MSCs were cultured in serum-free culture medium for 1 hr and then stimulated with 10 ng/mL PDGF-BB for 10 min. Furthermore, to determine whether PDGFR-β in MSCs is phosphorylated by co-culture with KM12SM cells, 2.0×10^5 MSCs in serum-free culture medium were plated into the lower chambers, and 2.0×10^5 KM12SM cells were cultured in a 6-well microchamber plate with uncoated inserts (0.4

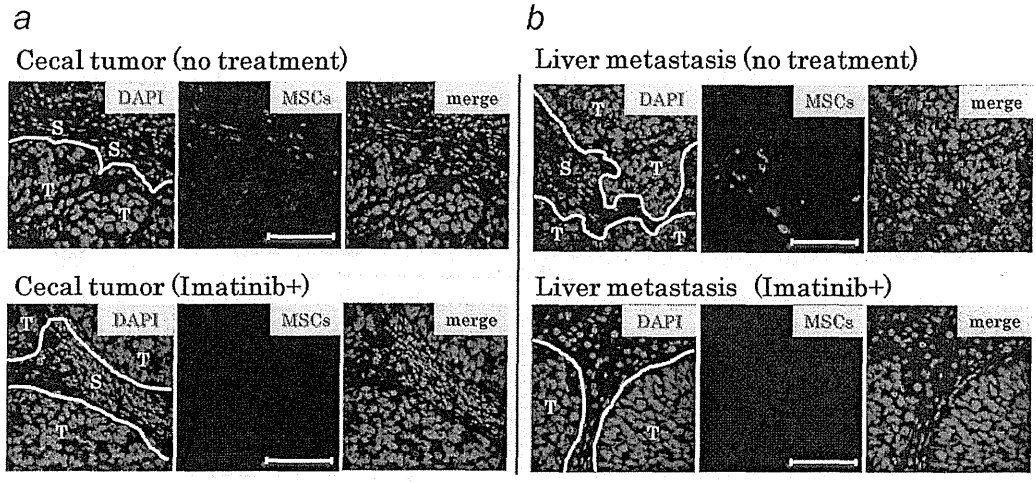

Figure 2. Migration of MSCs to orthotopic colon tumors and metastatic liver tumors. Systemically administered and PKH26-labeled MSCs (red) migrated to (*a*) the stroma of orthotopic colon tumors and (*b*) metastatic liver tumors. Imatinib treatment inhibited tumor-homing ability of MSCs *in vivo*. 4′,6-diamidino-2-phenylindole (DAPI) staining for cell nuclei (blue) shows outline of the stroma within tumor tissue. T: tumor nest, S: stroma, scale bars: 100 μm.

μm pore size, Corning Costar). After 24 hr, upper chambers containing KM12SM cells were set into the lower chambers in serum-free culture medium with or without 1 μM imatinib. After 1 hr of incubation at 37°C, inserts were removed. After 3 washes with cold phosphate-buffered saline containing 1 mmol/L sodium orthovanadate, MSCs were lysed. Unstimulated KM12SM cells were also lysed. Proteins (total protein 20 μg) were separated by SDS-PAGE and transferred to nitrocellulose transfer membranes (Whatman GmbH, Dassel, Germany). The immune complexes were visualized by enhanced chemiluminescence with an ECL Plus Kit (GE Healthcare, Buckinghamshire, UK).

Semiquantitative reverse transcription-polymerase chain reaction (RT-PCR)

Total RNA was extracted from gastric carcinoma cell lines with an RNeasy Kit (Qiagen, Tokyo, Japan) according to the manufacturer's instructions. RT-PCR was performed with the isolated RNA (1 μg). cDNA was generated from 1 μg of total RNA with a first-strand cDNA synthesis kit (Amersham Biosciences, Buckinghamshire, UK). Semiquantitative RT-PCR was performed with an AmpliTag Gold Kit (Roche, Mannheim, Germany) according to the manufacturer's instructions. RT-PCR reactions without reverse transcription showed no specific bands. Respective primer sequences, annealing temperatures, and PCR cycles were as follows: PDGFR-β forward, AGC TACCCCTCAAGGAATCATAG and PDGFR-β reverse, CTC TGGTGGATGGATTAAGACTG (PDGFR-β PCR product, 376 bp; 58°C; 30 cycles); and GAPDH forward, ATCATCCCT GCCTCTACTGG and GAPDH reverse, CCCTCCGACGC CTGCTTCAC (GAPDH PCR product, 188 bp; 58°C; 28 cycles); and PDGF-B forward, CGAGTTGGACCTGAAC ATGA and PDGF-B reverse, GTCACCGTGGCCTTCTTAAA (PDGF-B PCR product, 339 bp; 58°C; 30 cycles).

Statistical analysis

Values are expressed as mean ± standard error (SE). Survival curves were drawn by the Kaplan and Meier method, and the log rank test was used to analyze differences in survival rates. Student's- or Welch's *t*-test or the Wilcoxon test was used to analyze differences in other variables, as appropriate. Probability values of <0.05 were considered significant. All statistical analyses were performed with JMP software (SAS Institute, Cary, NC).

Results

Effect of imatinib on interaction between KM12SM cells and MSCs in vitro

RT-PCR and Western blotting revealed that MSCs expressed PDGFR-β and KM12SM cells expressed PDGF-B in culture conditions (Figs. 1*a* and 1*b*). PDGFR-β was expressed by MSCs but not by KM12SM cells, and phosphorylation of PDGFR-β in MSCs was completely inhibited by 1 μM imatinib (Fig. 1*b*). When the effects of imatinib on migration of MSCs were examined by migration assay, we found more MSCs migrated toward tumor cell culture than toward the medium without tumor cells; however, this effect was impaired with imatinib treatment (24.9 ± 2.5 *vs.* 43.4 ± 3.0 cells/field, $p < 0.05$; 9.3 ± 1.1 *vs.* 10.7 ± 1.1 cells/field) (Fig. 1*c*). We performed cell proliferation assay and confirmed that 1 μM imatinib did not affect cell proliferation of MSCs at least for 3 days (Fig. 1*d*).

To examine the effect of imatinib on the growth of KM12SM cells *in vitro*, cell proliferation assay was performed.

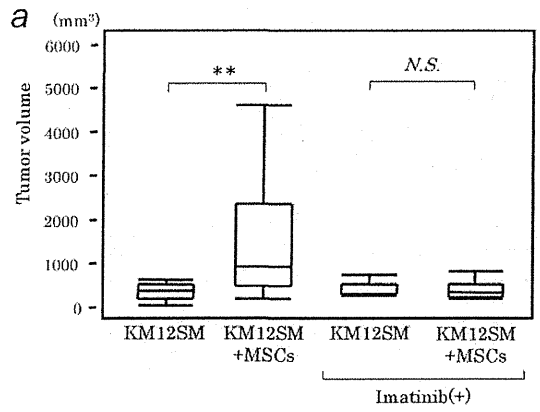

c

Implanted cells	No. of mice with liver metastasis/ total no. of mice
KM12SM	0/18
KM12SM+MSCs	2/10
KM12SM Imatinib(+)	0/8
KM12SM+MSCs Imatinib(+)	0/10

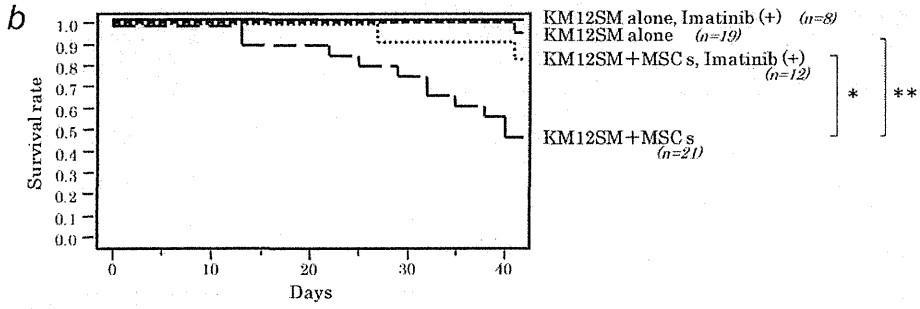

Figure 3. Comparisons of outcomes (cecal coinjection studies). Mice were divided into four groups according to the kind(s) of implanted cells and the treatment received, and mice surviving to day 42 were necropsied: (*i*) KM12SM cells alone without imatinib treatment (n = 18), (*ii*) KM12SM cells mixed with MSCs without imatinib treatment (n = 10), (*iii*) KM12SM cells alone with imatinib treatment (n = 8), or (*iv*) KM12SM cells mixed with MSCs with imatinib treatment (n = 10). (*a*) Transplantation of KM12SM cells mixed with MSCs (0.5×10^6:1.0×10^6, n = 10) resulted in significantly greater tumor volume than that resulting from transplantation of KM12SM cells alone (0.5×10^6, n = 18). Imatinib treatment impairs tumor promoting effect of MSCs (KM12SM cells alone, n = 8 mice; KM12SM cells with MSCs, n = 10 mice). $^{**}p < 0.01$, bars: SE. (*b*) Kaplan-Meier curves showing survival of mice bearing KM12SM cells alone (with or without imatinib treatment n = 8 or n = 19) and KM12SM cells mixed with MSCs (with or without imatinib treatment; n = 12 or n = 21). The survival rate was significantly lower in the mixed-cell group, and imatinib treatment significantly improved the survival rate in the mixed-cell group. $^{*}p < 0.05$, $^{**}p < 0.01$ (by log rank test). (*c*) Surviving mice were necropsied on day 42. The number of mice with liver metastasis is indicated. Macroscopic liver metastasis was seen only in the mixed-cell group that did not receive imatinib treatment.

The reported clinically effective plasma concentration of imatinib is 1 to 5 μM. The proliferation of KM12SM cells was not affected by imatinib treatment when the concentration of imatinib was increased up to 8 μM (Fig. 1*e*).

Imatinib inhibited MSC migration to orthotopic colon tumors and metastatic liver tumors

After injection of PKH-labeled MSCs into the tail veins of tumor-bearing mice, MSCs were detected specifically in the tumor stroma both at the primary site (colon) and the metastatic site (liver). In the imatinib treatment groups, no MSCs were detected in tumor stroma (Figs. 2*a* and 2*b*).

Imatinib inhibited tumor-promoting effect of MSCs in the orthotopic colon tumor model

The volumes of tumors resulting from transplantation of mixed cells was significantly greater than the volumes of tumors resulting from transplantation of tumor cells alone (511 ± 127 mm^3 *vs.* 1,478 ± 467 mm^3, $p < 0.01$). In the imatinib treatment groups, the tumor-promoting effect of MSCs was impaired (417 ± 61 mm^3 *vs.* 408 ± 67 mm^3) (Fig. 3*a*). The survival of mice was significantly lower in the mixed-cell group than in the group that received KM12SM cells alone ($p < 0.01$), and survival in the mixed-cell group that received imatinib was significantly improved ($p < 0.05$) (Fig. 3*b*). Macroscopic liver metastases were seen only in the mixed-cell group that did not receive imatinib (Fig. 3*c*). To clarify the mechanisms underlying the inhibitory effect of imatinib, we examined proliferation (PCNA-LI), apoptosis (AI), and angiogenesis (MVA) in primary tumors by immunohistochemistry. Between groups not given imatinib treatment, the PCNA-LI was significantly higher in the mixed-cell group than in the tumor-cell-alone group (30.6 ± 4.7 *vs.* 62.8 ± 4.6%, $p < 0.01$) (Fig. 4*a*), the AI was significantly lower in the mixed-cell group (7.2 ±